KSME

Springer

Journal of Mechanical Science and Technology 37 (2) 2023

Original Article
DOI 10.1007/s12206-023-0118-1

Keywords:
· Bi-directional valveless micropump
· Numerical simulation
· Coanda effect
· Piezoelectric effect
· Fluid deflector

Correspondence to:
Lipeng He
lipeng_he@126.com

Citation:
Zhang, Z., He, L., Zhou, J., Hu, D., Hou, Y., Cheng, G. (2023). A bi-directional valveless piezoelectric micropump based on the Coanda effect. Journal of Mechanical Science and Technology 37 (2) (2023) 749~755.
http://doi.org/10.1007/s12206-023-0118-1

Received March 4th, 2022
Revised July 16th, 2022
Accepted October 16th, 2022

† Recommended by Editor
Han Seo Ko

A bi-directional valveless piezoelectric micropump based on the Coanda effect

Zheng Zhang[1], Lipeng He[1], Jianwen Zhou[1], Dianbin Hu[1], Yi Hou[1] and Guangming Cheng[2]

[1]College of Mechanical and Electrical Engineering, Changchun University of Technology, Changchun 130012, China, [2]Institute of Precision Machinery and Smart Structure, Zhejiang Normal University, Jinhua 321004, China

Abstract In this paper, the hydrodynamic characteristics of a piezoelectric micropump operate on the Coanda effect, and the mechanism of bi-directional pumping are analyzed by numerical simulation and experiments. The research focuses on the different positions of the fluid deflector and the influence on the output of the micropump. The results show that a closer fluid deflector to the inlet can produce greater vortices in the suction process due to the Coanda effect, and the backflow diminishing is more significant as well. Moreover, the different positions of the fluid deflector can cause a phenomenon that the micropump will achieve bi-directional pumping. As a finding, vortices arranged in pairs could improve the rectification efficiency of the micropump. The micropump achieves a maximum flow rate of 40.5 ml/min and back pressure of 5.76 cmH_2o. In addition, the maximum flow rate per unit area can reach 305.2 μl/(min mm^2).

1. Introduction

As a key component of the microfluidic system, micropumps have been used in the fields of drug delivery systems [1], mechanical micro spray systems [2], portable fuel cells [3], and water cooling systems for chips [4]. In the last decades of development, various micropumps with piezoelectric, electrostatic, thermo-pneumatic [5], electroosmosis [6], and electromagnetic [7] actuators have emerged. Among them, the piezoelectric pump based on the principle of piezoelectric inverse effect has attracted the attention of researchers because of its small size, compact structure, rapid response, and no electromagnetic interference.

Generally, check-valves and no-moving-part valves [8-10] are used to direct fluids in the design of piezoelectric micropumps. The structure of the inlet and outlet tubes, chambers, and fluid deflector can all cause a difference in forward and reverse resistance in the valveless piezoelectric pump. Asymmetrical forward and reverse resistance can achieve the unidirectional flow of liquid. In contrast, valveless piezoelectric pumps are more reliable because of their low manufacturing cost, simple structure, and easy mounting. Most researchers' studies have been on diffuser/nozzle valveless micropumps [11].

The Coanda effect is a phenomenon in which the fluid tends to leave the original flow direction and flows alone on the protruding surface of an object. In this paper, a bi-directional valveless piezoelectric micropump based on the Coanda effect is proposed. The effects of five different fluid deflector positions on the hydrodynamic characteristics of the piezoelectric micropump and the mechanism of bi-directional pumping are analyzed by numerical simulation and experiments. Then, the experimental study is used to verify the numerical simulation results. It was found that vortices arranged in pairs could improve the rectification efficiency of the micropump and backflow diminishing is more significant as well. The micropump achieves a maximum flow rate of 40.5 ml/min and back pressure of 5.76 cmH_2o. In addition, the maximum flow rate per unit area can reach 305.2 μl/(min mm^2).

2. Design and operating principle

As shown in Fig. 1(a), the bi-directional valveless piezoelectric micropump based on the

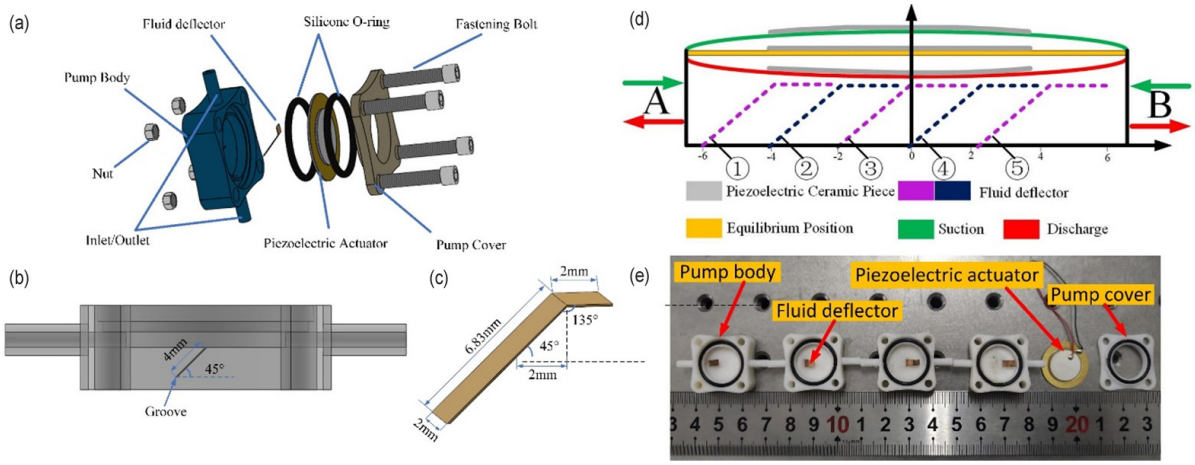

Fig. 1. (a) The structure of the micropump; (b) groove; (c) fluid deflector; (d) the working principle and the location of the fluid deflector; (e) prototype of the piezoelectric pump.

Coanda effect mainly consists of a pump body, a piezoelectric actuator, and a pump cover. The dimensions of the pump body are 23.7×23.7×8 mm^3 (L×W×H).

The diameter of the circular pump chamber is 15.2 mm, and the height is 2.5 mm. The inner and outer diameters of the inlet and outlet are 1.4 mm and 3 mm, respectively. The piezoelectric actuator consists of a ceramic chip (PZT-5) with a thickness of 0.2 mm and a brass substrate, where the diameter of the ceramic chip is 13 mm, and the diameter of the brass substrate is 20 mm. The silicone O-ring seals the working fluid, and the fastening bolts ensure the tightness of the entire pump. As shown in Fig. 1(b), a groove inclined at 45° is designed in the circular pump chamber with a length of 4 mm. The width and thickness of the groove are designed according to the size of the fluid deflector, which facilitates the installation of the fluid deflector. Fig. 1(c) shows the structure and dimensions of the fluid deflector, which has a thickness of 0.1 mm, an inclined beam of 6.83 mm, a horizontal beam with a length of 2 mm, and an angle of 135° between the two beams. A Makerbot 3D printer (Makerbot Replicator Mini+) of fused deposition modeling (FDM) was used to manufacture the piezoelectric micropump, and the material was polylactic acid (PLA). The material of the fluid deflector is beryllium bronze.

As shown in Fig. 1(d), the bending motion of the piezoelectric actuator consists of two processes in suction and discharge (green and red), the yellow part is the equilibrium position, and its amplitude is 0. The piezoelectric actuator vibrates upward to increase the volume of the pump chamber and decrease the chamber pressure in the suction mode. The piezoelectric actuator vibrates downward to decrease the volume of the pump chamber and increase the chamber pressure in the discharge mode. During this cycle, a positive net flow volume is generated in one of the outlet tubes due to the presence of a forward and reverse resistance difference in the pump chamber. At the same time, the piezoelectric actuator generates a continuous vibration, which achieves directional pumping of the fluid at a macroscopic level. Fig. 1(e) shows the prototype of the piezoelectric pump.

3. Numerical simulation

In general, the fluid herein is assumed to be an incompressible fluid. The set of equations solved by ANSYS CFX is the unsteady Navier-Stokes equations in their conservation form. To obtain solutions for real flows, a numerical approach must be adopted whereby the equations are replaced by algebraic approximations that can be solved using a numerical method. ANSYS CFX uses an element-based finite volume method, which involves discretizing the spatial domain using a mesh. After discretizing the volume and surface integrals, the integral equations become (ANSYS CFX software: Help. Version 18, n.d.):

$$V\left(\frac{\rho-\rho^0}{\Delta t}\right)+\sum_{iP}\dot{m}_{iP}=0\,, \tag{1}$$

$$y=\beta_0+\sum_{i=1}^{n_d}\beta_i x_i+\sum_{i=1}^{n_d}\sum_{j\geq i}^{n_d}\beta_{ij}x_i x_j\,,$$

$$\sum_{iP}\left[u_{eff}\left(\frac{\partial\vec{U}_i}{\partial y_j}+\frac{\partial\vec{U}_j}{\partial x_i}\right)\Delta n_j\right]_{ip}+\overline{S_{\vec{U}_i}}V\,, \tag{2}$$

$$V\left(\frac{\rho\varphi-\rho^0\varphi^0}{\Delta t}\right)+\sum_{ip}\dot{m}_{ip}\varphi_{i_P}=$$

$$\sum_{ip}\left(\Gamma_{eff}\frac{\partial x}{\partial x_j}\Delta n_j\right)_{i_P}+\overline{S_\varphi}V \tag{3}$$

where V refers to volume and Δn_j refers to the discrete outward surface vector. Where $\dot{m}_{iP}=\left(\rho\vec{U}_j\Delta n_j\right)_{ip}$, $\dot{m}$ refers to mass flow rate. U_i refers to the discrete velocity vector, Δt refers to the time step. The subscript ip represents evaluation at an integration point and the superscript ° refers to the old time level. The p' refers to the pressure, u_{eff} refers to the effective dynamic viscosity, φ refers to a generalized

variable, and S_φ is a generalized source term corresponding to φ.

Where v' indicates the constant incoming flow velocity. l represents pipe length and u represents fluid viscosity. Here, the dimensionless parameter Reynolds number is expressed as:

$$R_e = \frac{\rho v' l}{u}. \tag{4}$$

The flow is usually assumed to be laminar. In addition, the working fluid is water at 25 °C with no roughness and other surfaces with non-slip boundary conditions. The type of analysis is transient analysis. High-resolution format and second order backwind Euler are used to advection scheme and implicit time-step method, respectively. The convergence condition is set to a maximum root mean square (RMS) of less than 1.0E-4.

Mesh quality and mesh independence play an important role in the accuracy of the computational hydrodynamic results. In order to exclude the influence of mesh density on the computational results. The mesh independence check was tested before the numerical simulation, as shown in Fig. 2(b). Considering the selection from the accuracy and economy of calculation, the number of grids is 2525540 for calculation. The time step not only determines the resolution of the calculation time and the stability of the calculation but also affects the grid independence in transient calculations. The time step is generally estimated using Courant number:

Table 1. Independent analysis of grids.

Number of 3D grids (10^4)	Flow resistance coefficient	Deviation (%)
6.4892	0.36945	2.68
25.8436	0.35952	1.99
50.3763	0.35234	0.63
100.8145	0.35012	4.4
159.7131	0.33446	3.26
200.1435	0.34463	3.01
252.5540	0.33426	1.11
399.3727	0.33052	0.002
450.2122	0.33043	0.001
512.7231	0.33054	0.002
630.7322	0.33049	\

$$C = \frac{v_c \times \Delta t_c}{\Delta x_c} \tag{5}$$

where v_c is the characteristic flow velocity of the fluid, Δt_c is the time step, and Δx_c is the length of the edge of the local finite volume mesh cell. The courant number represents the the number of meshes that the fluid passes through in a one-time step. In this study, a time step of 8.3E-4 s was shown to be sufficient for the transient calculation.

To investigate the relationship between the position of the fluid deflector and its influence on the hydrodynamic characteristics of the micropump, in ANSYS computational fluid X (CFX), the pressure by inlet is set to 50, 100, 200, 300, 400 Pa, respectively, and the relative pressure at the outlet is 0 Pa, the reference pressure is 1 atm. The fluid flows from the inlet to the outlet and then from the outlet to the inlet to simulate the magnitude of fluid resistance at different pressure drops. It should be noted that the average speed v here is calculated by the CFD-post-function calculator.

Fig. 2(c) shows the numerical simulation results of flow from A to B and from B to A under different pressure drops. It can be seen that the flow of pumps ①, ②, and ③ from A to B is greater than the flow from B to A, and the flow of pumps ④ and ⑤ from B to A is greater than the flow from A to B. Fig. 2(d) shows numerical simulation results of the net flow resistance difference from A to B at different pressure drops. The flow resistance difference of pump ①, pump ②, and pump ③ from A to B is negative. Figs. 2(c) and (d) show that the fluid flows forward from A to B, where A is the inlet and B is the outlet. The net resistance of pump ④ and pump ⑤ from A to B is positive, which proves that they flow from B to A in a positive direction, where B is the inlet and A is the outlet. To investigate the performance of the micropump and the internal flow field when the fluid deflector is set at five different positions, the velocity streamlines of the micropump are simulated for both flow directions at a pressure difference of 200 Pa, and the number of streamlines is set to 500. As shown in Figs. 3(a)-(e), the subscript of 1 means that the flow direction is from A to B, and two vortices are generated in the pump chamber. As the fluid deflector is set close to B, the intensity of the vortex increases as more fluid flows into the cyclonic vortex. The subscript of 2 represents the flow from B to A, and four vortices are generated in the pump cavity, from the results it is clear that as

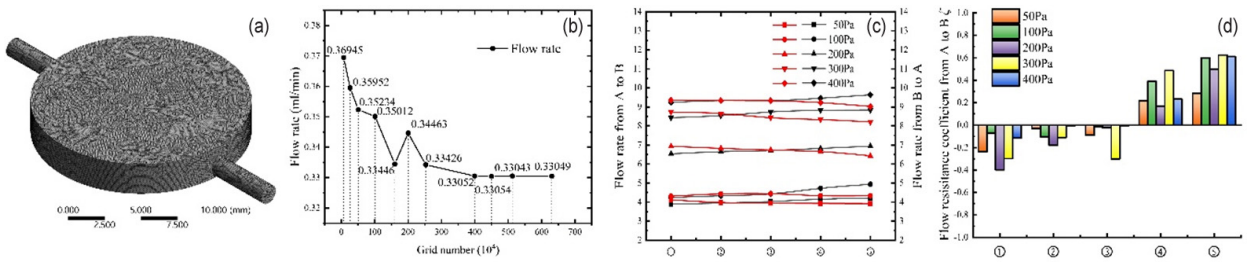

Fig. 2. (a) Meshing; (b) grid independence check; (c) simulation results of flow rate; (d) simulation results of net flow resistance coefficient.

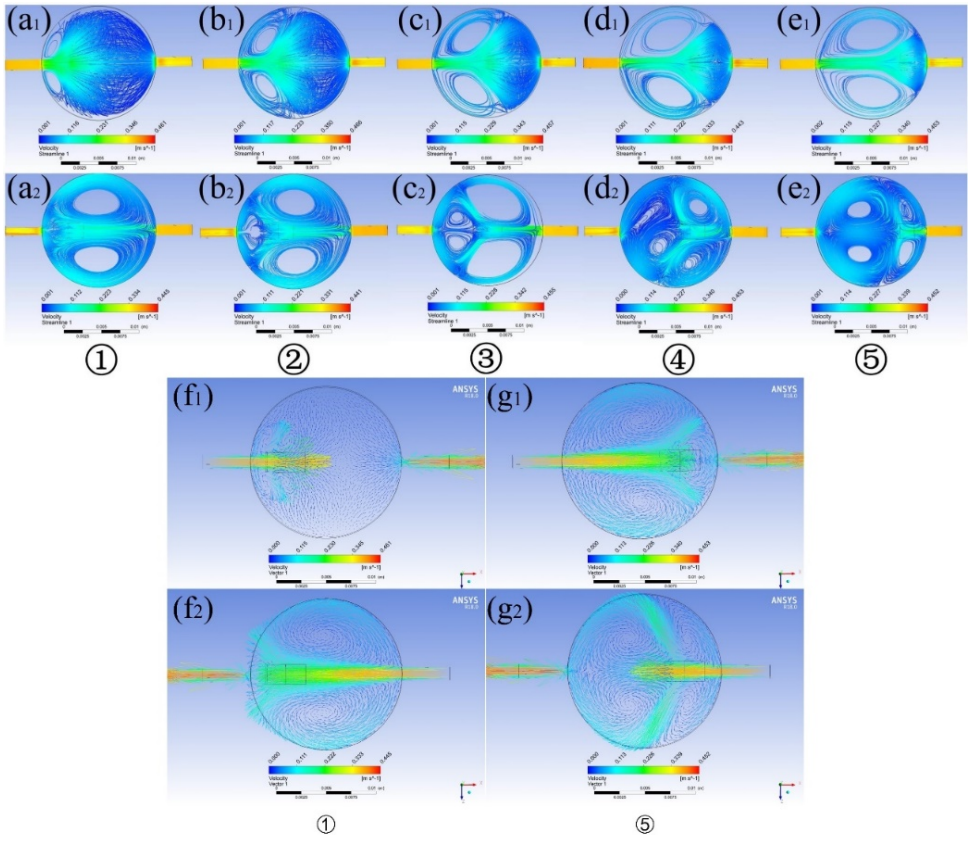

Fig. 3. (a)-(e) Velocity streamline; (f) and (g) vector flow rate.

the fluid deflector moves toward B, two vortices near A gradually enlarge and the vortex near B gradually reduce.

In order to obtain the flow direction of the fluid in the pump chamber, the pump body ① and ⑤ are vector velocity processed, and the arrows on the surface were set to 2000, the results are shown in Figs. 3(f) and (g). Fig. 3(f_1) shows the forward vector velocity streamlines (from A to B) for pump ①. Most fluid flows along the inner wall of the pump chamber to the outlet based on the Coanda effect, but a small vortex is generated at the inlet after the fluid passes through the fluid deflector, and blocks a portion of the fluid. Fig. 3(f_2) shows the vector streamline diagram from the outlet to the inlet in pump ①. When the fluid passes through the fluid deflector, most of the fluid hits the inner wall of the pump chamber to produce counterflow and vortex, reducing the backflow phenomenon. Similarly, Fig. 3(g_2) shows the forward vector velocity streamline of pump ⑤ (from B to A), where the fluid hits the fluid deflector and flows along the inner wall to the outlet. Fig. 3(g_1) shows the reverse flow velocity vector diagram of pump ⑤. Most of the fluid flows in the opposite direction and produces a vortex, a small part of the flow to the outlet after the fluid flows through the fluid deflector and hits the inner wall.

From the research above, the inlet of micropump ①, ②, ③ is A and the inlet of micropump ④, ⑤ is B. It is clear that the pumping mechanism of the micropump is: micropump ①, ②, ③ use the Coanda effect to generate vortices to reduce backflow, just like Fig. 3(f_2). Micropumps ④ uses vortices to reduce backflow, just like Fig. 3(g_1). In Fig. 3(g_2), micropump ⑤ produces two big vortices in the center of the chamber and two other small vortices along the inner wall of the pump chamber, the big vortex and the small vortex on the one side of the chamber are in opposite directions, and the flow rate of the fluid between those two vortices are increased to produce a positive effect to push the fluid flowing from B to A.

4. Experiment

In this paper, the performance of the bi-directional pumps under different structural conditions is evaluated and discussed based on the experimental test system shown in Fig. 4, to provide data references for the micropumps in production and practical applications. In the experiments, five micropumps with different positions of fluid deflector are fabricated and discussed. It should be noted that pump ③ did not generate a performance curve due to the small difference in forward and reverse flow resistance based on the existing experimental preparation conditions and experimental test system, and the pump body could not overcome the working resistance during the flow. Therefore, the output characteristics of pump ③ are not expressed and discussed in this paper. The possible reasons are: (1) there are inlet losses and outlet pipe losses at the outlet pipe of the pump; (2) the piezoelectric actuator must

overcome the surface tension of the fluid in order to discharge the fluid into the pump chamber; (3) PLA material has a certain roughness, and the flow of fluid will generate energy loss.

The flow rate variation curves of the micropump ① are shown in Fig 4(b). the maximum flow rate is achieved at 60 Hz with the highest flow rate of 24.9 ml/min. At the same frequency, the flow rate of the micropump gradually increases as the pump voltage increases. Fig. 4(c) shows the flow rate variation curve of the micropump ②. The flow rate and effective flow range of the micropump ② increase with the increase of the voltage. At the same time, the optimal frequency increases with an increasing voltage, for the fluid deflector is influenced by the piezoelectric actuator and vibrating. The micropump ② shows a high flow rate at 140 V-50 Hz, 160 V-55 Hz, 180 V-60 Hz, and 200 V-65 Hz, respectively. The maximum flow rate reaches 14.3 ml/min at 200 V-65 Hz. In contrast, the overall flow rate and the range of effective frequencies of the micropump ② are lower than the flow rate of the micropump ①. The Coanda effect sucks in the surrounding fluid, due to the existence of the sidewall, the peripheral high-pressure area of the medium is too late to add in, and the pressure on the side of the smaller differential will be lower than the side of the larger differential, resulting in the fluid is pushed to the side of the smaller differential.

The flow rate variation curve of the micropump ④ and the micropump ⑤ are shown in Figs. 4(d) and (e), respectively. The optimal frequency of the micropump ④ is 75 Hz, and the maximum flow rate is 28.5 ml/min. The optimal frequency of the micropump ⑤ is 110 Hz, and the maximum flow rate is 40.5 ml/min. In conclusion, the flow rate and effective frequency range of micropump ⑤ are better than the other micropumps. Overall, the position of the fluid deflector has a significant impact on the overall performance of the pump. The closer the fluid deflector to the inlet of the micropump, the better the flow rate is.

Fig. 4(f) shows the curves of back pressure with driving frequency for the four micropumps at 200 V. The maximum back pressures of the four micropumps are 3.86, 1.9, 4.26, and 5.76 cmH2o, obtained at 75, 80, 125, and 145 Hz, respectively. It can be inferred that vortices arranged in pairs of the micropump ④ and ⑤ could improve the back pressure and rectification efficiency of the micropump.

By testing the flow and pressure characteristics of the experimental prototype, Figs. 4(e) and (f) is used to evaluate the efficiency of the micropumps [12, 13]. At a voltage of 200 V, the pump efficiency is shown in Fig. 4(g).

Table 2. Performance comparison of this pump with reported bi-directional pumps.

Reference	Rectifying principle	Drive mechanism	Drive voltage (V)	Maximum flow rate (ml/min)	Maximum flow per unit area μl/(min mm^2)
Wijngaart [14]	Change of pumping frequency	Piezoelectric	125	0.03	1.1
Hayamizu [15]	Driving waveform	Piezoelectric	100	0.02	15.3
Lee [16]	Chamber arrangement	Piezoelectric	120	0.012	0.02
Yoon [17]	Oblique channels	Piezoelectric	385	0.32	3.2
Chee [18]	Dynamic rectifying	Electromagnetic	19.6	1.52	53.8
Yang [19]	Regulating the voltage	Piezoelectric	300	0.408	0.832
This work	Coanda effect	Piezoelectric	200	40.5	305.2

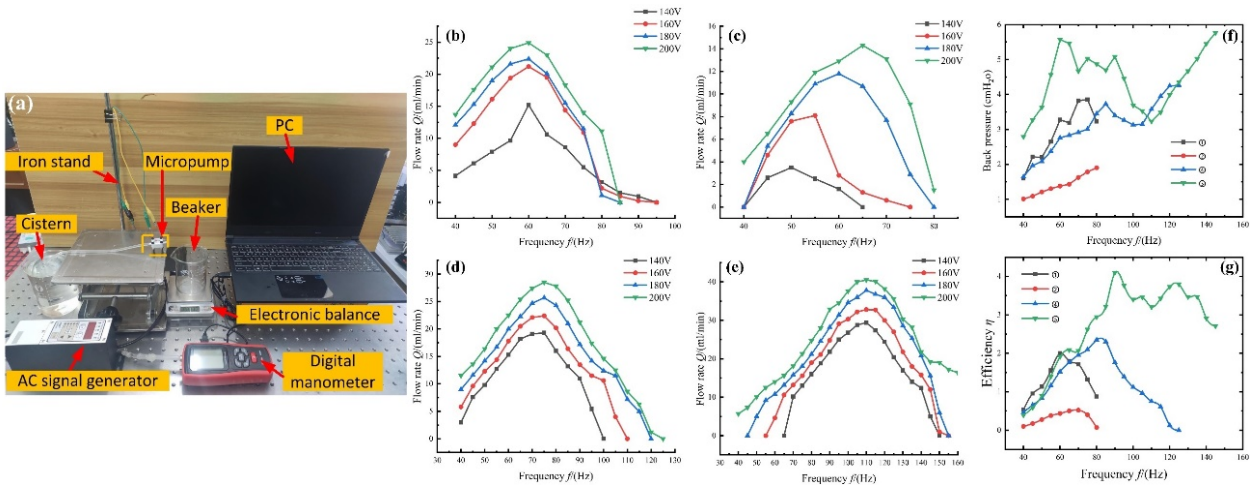

Fig. 4. (a) Performance test experimental system. Flow rate of (b) pump ①; (c) pump ②; (d) pump ④; (e) pump ⑤; (f) relationship between back pressure and frequency; (g) efficiency.

In order to have a better understanding of the performance improvement of the bi-directional micropump, it is compared with the previous bi-directional micropump, and the results are shown in Table 2. Chee et al. proposed a new bi-directional pumping principle based on a dynamic rectification mechanism, but the electromagnetic micropump has the defects of being too large and is not stable in the electromagnetic interference. In this research and the presented work by the Wijingaart et al., Hayamizu et al., Lee, Yoon et al. and Yang et al., we all use piezoelectricity as the driving mechanism. The miniature size of the piezoelectric pump is a significant advantage, which makes the piezoelectric pump becoming an increasingly common choice. Compared with other work, this paper takes an advantage of the mechanism based on the Coanda effect to obtain a significant performance improvement. The flow rate per unit area pumped is an extremely important performance indicator for micropumps.

5. Conclusions

This paper is to study the hydrodynamic characteristics of the micropump brought by the Coanda effect by numerical simulation and experiments. The effects of five different fluid deflector positions on the hydrodynamic characteristics of the piezoelectric micropump and the mechanism of bi-directional pumping are investigated. Experiments are used to validate the proposed numerical model and the possible reasons for the differences between experimental and numerical simulation results. The results show that:

1) Numerical simulations illustrate that the micropumps operate under the Coanda effect, which is generated by the flow and the fluid deflector, also vortices are produced to suppress the backflow phenomenon of the liquid and achieve bi-directional pumping of the micro-pump.

2) As a finding, the flow rate of the fluid between those two vortices arranged in pairs is increased to produce a positive effect to push the fluid flowing. That could improve the rectification efficiency of the micropump.

3) Experiments show that the micropump can reach a maximum flow rate of 40.5 ml/min, and a maximum back pressure of 5.76 cmH_2o. The flow rate per unit area of the pump is higher than the reported bi-directional micropumps.

Acknowledgments

This work was supported by the National Natural Science Foundation of China (51805489), and the China Scholarship Council (202008220173).

References

[1] J. T. Wang et al., A resonant piezoelectric diaphragm pump transferring gas with compact structure, *Micromachines*, 7 (12) (2016) 219.

[2] A. Kacar, M. B. Oozer and Y. Tascioglu, A novel artificial pancreas: energy efficient valveless piezoelectric actuated closed-loop insulin pump for T1DM, *Applied Sciences-Basel*, 10 (15) (2020) 5294.

[3] A. S. Yang et al., Design and analysis of a valveless impedance pump for a direct sodium borohydride-hydrogen peroxide fuel cell, *Journal of Electrochemical Energy Conversion and Storage*, 17 (3) (2020) 031009.

[4] Y. L. Zhang et al., Design of micro-displacement amplifier for the micro-channel cooling system in the micro-pump, *Forschung Im Ingenieurwesen-Engineering Research*, 84 (2) (2020) 161-168.

[5] C. H. Yang et al., Thermopneumatic suction integrated microfluidic blood analysis system, *PLoS ONE*, 14 (3) (2019) e0208676.

[6] S. Waheed, S. Noreen and A. Hussanan, Study of heat and mass transfer in electroosmotic flow of third order fluid through peristaltic microchannels, *Applied Sciences-Basel*, 9 (10) (2019) 2164.

[7] D. M. Zhu et al., Design and experimental verification on characteristics of electro-hydraulic pump, *Mechanical Systems and Signal Processing*, 144 (2020) 106771.

[8] X. H. He et al., A bidirectional valveless piezoelectric micropump with three chambers applying synthetic jet, *Journal of Mechanical Science and Technology*, 30 (9) (2016) 4015-4022.

[9] R. K. Haldkar, V. K. Gupta and T. Sheorey, Modeling and flow analysis of piezoelectric based micropump with various shapes of microneedle, *Journal of Mechanical Science and Technology*, 31 (6) (2017) 2933-2941.

[10] Y. M. Na, H. S. Lee and J. K. Park, Fabrication and experiment of piezoelectric pump imitating peristalsis, *Journal of Mechanical Science and Technology*, 32 (10) (2018) 4737-4745.

[11] X. H. He, C. M. Shan and H. Yang, Research and verification of similar laws in valveless piezoelectric micropumps, *Micro and Nano Letters*, 16 (5) (2021) 281-289.

[12] J. Huang et al., Development and performance comparison of valveless piezoelectric pumps with asymmetrical channels, *Sensors and Actuators A-Physical*, 314 (2020) 112241.

[13] Y. K. Yin et al., Design and investigation on a novel piezoelectric screw pump, *Smart Materials and Structures*, 29 (8) (2020) 085013.

[14] W. van der Wijngaart et al., The first self-priming and bi-directional valve-less diffuser micropump for both liquid and gas, *Proc. IEEE Thirteenth Annual International Conference on Micro Electro Mechanical Systems* (2000) 674-679.

[15] S. Hayamizu et al., Development of a bi-directional valve-less silicon micro pump controlled by driving waveform, *Sensors and Actuators A: Physical*, 103 (1) (2003) 83-87.

[16] D.-S. Lee, J. S. Ko and Y. T. Kim, Bidirectional pumping properties of a peristaltic piezoelectric micropump with simple design and chemical resistance, *Thin Solid Films*, 468 (1-2) (2004) 285-290.

[17] J. S. Yoon et al., A valveless micropump for bidirectional applications, *Sensors and Actuators A: Physical*, 135 (2) (2007) 833-838.

[18] P. S. Chee et al., Bidirectional flow micropump based on dynamic rectification, *Sensors and Actuators A-Physical*, 204 (2013) 107-113.

[19] S. Yang et al., A bidirectional valveless piezoelectric micropump with double chambers based on Coanda effect, *Journal of the Brazilian Society of Mechanical Sciences and Engineering*, 38 (2) (2016) 345-353.

Lipeng He is currently a Lecturer of School of Mechatronic Engineering, Changchun University of Technology, China. He received his Ph.D. degree from the Mechatronics Engineering of Jilin University, China in 2010. His research focuses on piezoelectric pump, piezoelectric actuators and energy harvesting.